Journal of Alloys and Compounds 696 (2017) 619–626

Contents lists available at ScienceDirect

Journal of Alloys and Compounds

journal homepage: http://www.elsevier.com/locate/jalcom

Eu^{3+} doped tellurite glass ceramics containing SrF_2 nanocrystals: Preparation, structure and luminescence properties

Michalina Walas [a, *], Tomasz Lewandowski [a], Anna Synak [b], Marcin Łapiński [a], Wojciech Sadowski [a], Barbara Kościelska [a]

[a] Faculty of Applied Physics and Mathematics, Department of Solid State Physics, Gdańsk University of Technology, ul. Gabriela Narutowicza 11/12, 80-233 Gdańsk, Poland
[b] Institute of Experimental Physics, Faculty of Mathematics, Physics and Informatics, University of Gdańsk, ul. Wita Stwosza 57/246, 80-952 Gdańsk, Poland

ARTICLE INFO

Article history:
Received 9 August 2016
Received in revised form
9 November 2016
Accepted 21 November 2016
Available online 22 November 2016

Keywords:
Glass ceramics
Luminescence
Eu^{3+}
SrF_2 nanocrystals

ABSTRACT

Eu^{3+} doped tellurite glass ceramics containing SrF_2 nanocrystals were prepared using melt quenching technique and subsequent heat treatment of glass in 370 °C for different time periods. Thermal properties of glass matrix have been determined based on DSC measurements. XRD and XPS results confirmed formation of SrF_2 nanocrystals in glass matrices after annealing at 370 °C. FTIR studies revealed absorption bands in the range of 500–850 cm^{-1} characteristic to TeO_2 glasses. Obtained materials exhibited emission originated from the ^5D_J ($J = 0–2$) to the ^7F_J ($J = 0–4$) transitions of Eu^{3+} ions under 395 and 465 nm excitations. TRES measurements indicated presence of two different surroundings of the Eu^{3+} ions. In glass ceramics samples longer lifetimes of 615 nm emission of Eu^{3+} were achieved in comparison to the precursor glass.

1. Introduction

Glass ceramics containing RE^{3+} (RE = rare earth ions) have been widely investigated in past decades due to their possible applications in solid-state lasers, fiber amplifiers, light emitting diodes, 3D displays etc. [1]. Among them, transparent oxyfluoride glass ceramics containing fluoride nanocrystals doped with RE^{3+} ions have attracted considerable attention. In such materials, fluoride nanocrystals enriched with RE^{3+} are homogeneously embedded in oxide glass matrix [2]. Due to much smaller size of nanocrystals than the visible light wavelength and similar refractive indices between them and glass matrix, glass ceramics are characterized by high transparency in visible and near infrared region [3]. Additionally, oxyfluoride glass ceramics can be prepared using simple melt-quenching technique followed by a heat treatment, during which crystallization of fluoride phase takes place [4].

Most of the research focused on development of transparent tellurite based glass ceramics containing fluoride crystalline phases such as PbF_2 or CdF_3 in the glass matrices [5–7]. However, these glass ceramics contain toxic lead and cadmium fluoride raw materials, so they cannot be used extensively due to environmental concerns. For this reason, the glass ceramics containing REF_3 (RE = La or Y) and MF_2 (M = Ca, Sr and Ba) nanocrystals became a subject of intensive research [8–15]. The alkaline-earth fluorides provide low phonon energy and large transfer coefficient between RE^{3+} ions in the crystal lattice, which can improve optical properties without a loss of transparency [16]. They are also more environmentally friendly than lead and cadmium compounds. Studies mostly included silica-based oxyfluoride glass ceramics. For example, luminescence of europium in $50SiO_2$-$22Al_2O_3$-$20SrF_2$-6NaF-$2EuF_3$ glass ceramics have been investigated by Luo et al. [17]. Recently, Imanieh et al. [18] synthesized transparent aluminosilicate glass ceramics containing Er^{3+}, Yb^{3+}:$Sr_{1-x}Y_xF_{2+x}$ nanocrystals. In this case, efficient upconversion luminescence process took place.

However, there is limited number of reports on the tellurite-based glass ceramics containing fluoride nanocrystals doped with RE^{3+} ions. Transparent glass ceramics with $32TeO_2$-$15SiO_2$-$28AlF_3$-15CaO-10NaF-$1.5ErF_3$ composition, containing CaF_2 nanocrystals were successfully synthesized by Zhao-xia Hou et al. [19]. CaF_2 crystalline phase was obtained by controlled heat-treatment at 370 °C nucleation for 4 h and crystallization at 420 °C for 6 h.

In this paper, we have successfully prepared the Eu^{3+} doped TeO_2-BaO-Bi_2O_3 tellurite-based glass ceramics containing SrF_2

* Corresponding author.
E-mail address: mwalas@mif.pg.gda.pl (M. Walas).

http://dx.doi.org/10.1016/j.jallcom.2016.11.301
0925-8388/

nanocrystals. The size of SrF_2 crystallites has been controlled by the change of heat treatment duration. Structural and luminescence properties of prepared glass ceramics were studied in detail and results proved incorporation of Eu^{3+} into SrF_2 lattice as well as luminescence intensity variation depending on SrF_2 crystallites size. To our best knowledge, such glass ceramics systems have never been reported before.

2. Experimental (materials and methods)

Tellurite based glasses with the nominal composition (in mol%) $73TeO_2$-$4BaO$-$3Bi_2O_3$-$18SrF_2$-$2Eu_2O_3$ were synthesized using conventional melt quenching technique. Well mixed starting raw materials (TeO_2, $BaCO_3$, $Bi_5OH(OH)_9(NO_3)_4$, SrF_2 and $Eu(NO_3)_3$ were decomposed at 600 °C for an hour and melted in porcelain crucible at 800 °C for 0.5 h; after that time the temperature was reduced to 700 °C for another 0.5 h. Melts were poured onto preheated steel plate and pressed by another plate immediately; then cooled down to the room temperature. Two series of glass ceramic samples were obtained by heat treatment of precursor glass (PG) at 360 °C and 370 °C for different time periods (series labelled as GC360 and GC370 in Table 1). Each step of glass and glass ceramics synthesis was carried out in air atmosphere.

Structural properties of samples were investigated using several techniques. X-ray diffraction measurements (XRD) were carried out to confirm the lack of long range order in the as-prepared glass samples and to determine crystalline structure of obtained glass ceramics. Measurements were performed on powder samples on Philips X'PERT PLUS diffractometer with Cu-Kα radiation ($\lambda = 0.154$ nm). The size of the SrF_2 crystallites was estimated based on XRD data using Scherrer's equation. Differential scanning calorimetry (DSC) measurements were executed on Netzsch Simultaneous TGA-DSC, STA 449 F1 in platinum-rhodium crucible in air atmosphere with the heating rate of 10 K/min. DSC results allowed to characterize the thermal properties of the as-prepared glass sample: glass transition temperature T_g and crystallization peak temperature T_c. Fourier transform infrared spectroscopy (FTIR) measurements were carried out on Perkin-Elmer Frontier MIR/FIR spectrometer with TGS detector in order to determinate the types of chemical bonds in the structural units present in the samples. The measurements were performed on pellet samples mixed with potassium bromide KBr in weight ratio (Sample: KBr) 1:100. The spectra were obtained in the mid-infrared range. X-ray Photoelectron Spectroscopy analysis (XPS) was carried out with X-ray photoelectron spectrometer (Omnicron NanoTechnology) with 128-channel collector. Investigated samples were pre-cleaned by Ar ion beam. XPS measurements were performed in an ultra-high vacuum conditions, below 1.1×10^{-8} mBar. The photoelectrons were excited by an Mg-Kα X-ray source with X-ray anode operated at 15 keV and 300 W. The absorption spectra of glass and glass-ceramics samples were measured using Perkin-Elmer Lambda 35 UV–Vis spectrophotometer. Luminescence emission and excitation spectra of precursor glass and glass ceramics samples were collected by Perkin Elmer LS 55 fluorescence spectrometer using pellet samples mixed with KBr in weight ratio 1:1. Time-resolved emission spectra (TRES) were obtained with the employment of pulsed spectrofluorometer designed in our laboratory and described earlier in detail [20]. The laser system PL 2143A/SS with Nd:YAG laser and the PG 401/SH optical parametric generator emitting pulses of FWHM ≈ 30 ps from EXSPLA, was used as the excitation light source. The emission signal was analyzed by a Bruker Optics 2501S spectrometer and the Hammamatsu streak camera C4334-01 model. All operations are fully automated and controlled by the original Hamamatsu HPDTA software which allows for the real-time data analysis. The single measurement results are obtained as a quasi-three-dimensional, colorful flat image, with the wavelength in horizontal axis, the time in vertical axis and the intensity expressed by a range of colors. By slicing the streak camera image at a certain time interval, the time decays are obtained [16]. All measurements except of DSC were carried out at room temperature.

Table 1
Designation of the glass ceramics and heat treatment parameters.

Samples series	Heat treatment temperature (°C)	Heat treatment time (h)
GC360	360	0.5
		1.0
		1.5
		24.0
GC370	370	0.5
		1.0
		1.5
		3.0
		4.0
		6.0
		7.0
		9.0
		12.0
		24.0

3. Results and discussion

3.1. DSC analysis

In order to analyze the thermal properties as well as the thermal stability of the precursor glass, the DSC measurements were performed. DSC result of the TeO_2-BaO-Bi_2O_3-SrF_2 oxyfluoride glass specimen is shown in Fig. 1. One can observe the glass transition temperature (T_g) at 348 °C, the crystallization peak temperature (T_c) at 382 °C and the melting temperature (T_m) at 520 °C. The onset of crystallization peak temperature (T_x) was located at 375 °C. The glass thermal stability ΔT has been evaluated as a difference between T_x and T_g: $\Delta T = T_x - T_g$. The value of ΔT in case of TeO_2-BaO-Bi_2O_3-SrF_2 sample equaled 27 °C. Additionally, Saad-Poulain (S) and Hruby (H) parameters were estimated to further investigation of the thermal properties in precursor glass system. The thermal stability S parameter describes the glass resistance against devitrification and it is defined as [21]:

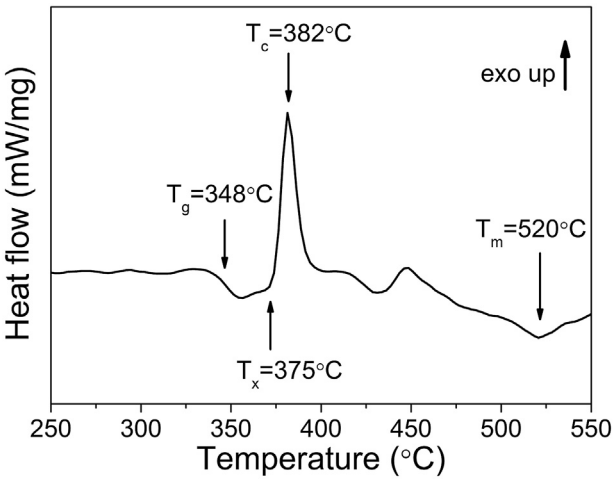

Fig. 1. DSC curve of glass matrix.

$$S = (T_c - T_x)(T_c - T_g)/T_g$$

It takes into account the width of the devitrification peak $(T_c - T_x)$ the large value of which delays the nucleation process. In studied precursor glass system, the calculated value of S = 0.68. For other tellurite glass systems, for example [22] S parameter equaled 6.89 and 11.36, whereas in case of fluorozirconate-based glass ceramics with BaF_2 nanocrystals [23] the S value was in the range of 0.33–0.44. The parameter H is characterizing the tendency to form glass and involves the glass transition temperature T_g, the melting temperature T_m and the crystallization temperature T_c [24]:

$$H = (T_c - T_g)/(T_m - T_c)$$

Typical H values ranged from 0.1 to 2.0 for good glass forming systems. In present study, the H = 0.25, suggesting relatively high tendency of crystallization in the TeO_2-BaO-Bi_2O_3-SrF_2 glass ceramics which could be mainly caused by the 18 mol% addition of SrF_2 into precursor glass matrix. However, it might be considered as an advantage in terms of preparation glass ceramics from the precursor glass.

Formation of the crystalline phase in glass matrix is considered to be strongly dependent on the temperature and time of the heat treatment procedure [25]. In order to achieve nanosized crystallites, the heat treatment temperatures were selected in the range of several degrees above the determined T_g and slightly below the T_x. Due to this fact, two temperatures: 360 and 370 °C were used to obtain SrF_2 nanocrystalline phase. Additionally, different times were taken into account for both temperatures.

3.2. XRD analysis

XRD diffraction analyses were carried out in order to investigate the structure of prepared samples. Fig. 2 shows the XRD patterns of Eu^{3+} doped precursor glass and two series of glass ceramics samples heat treated at 360 and 370 °C for different time periods. The diffraction pattern of the glass specimen (Fig. 2.) showed only the broad amorphous halo characteristic to the presence of short range order in glass matrix. The similar situation occurs in case of samples heat-treated at 360 °C in 0.5, 1.0, 1.5 and 24.0 h. The XRD patterns of these samples did not contain diffraction peaks but only the amorphous halos indicating that at 360 °C the heat treatment process did not result in the crystallites formation. On the other hand, the diffraction patterns of the specimens heat treated at 370 °C (Fig. 3.) revealed several sharp diffraction peaks arisen on the amorphous halo suggesting successful growth of crystalline

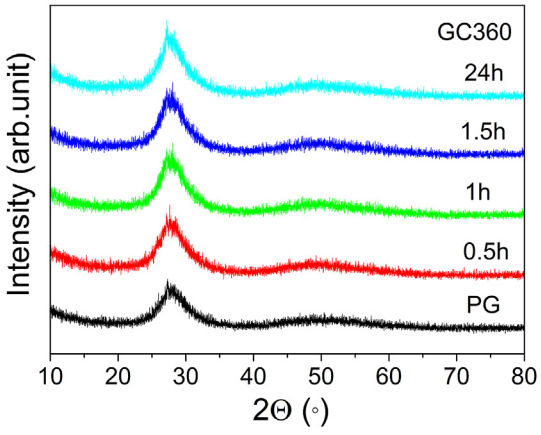

Fig. 2. XRD pattern of PG and GC360 series.

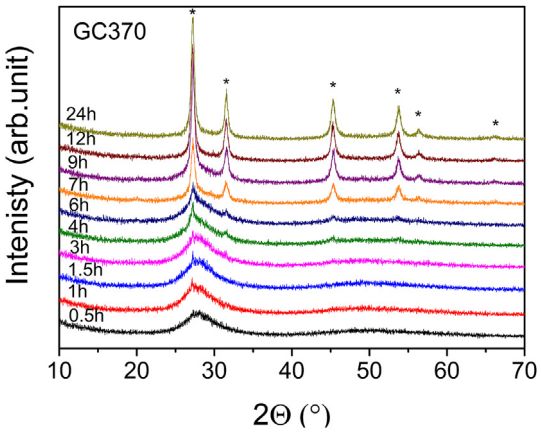

Fig. 3. XRD pattern of GC370 series.

phase. The intensity of the diffraction peaks enhanced gradually with increasing of the heat treatment procedure time indicating the improved crystallinity. All observed peaks matched very well with the JCPDS No. 86–2418 which corresponded to SrF_2 cubic structure with the space group Fm3m (225). The average crystallite size (D) of the SrF_2 crystalline phase in glass ceramics samples was evaluated for each sample from the most intensive diffraction peaks (111), (200), (220) and (311) following the Scherrer's equation:

$$D = (K * \lambda)/(\beta * \cos \Theta)$$

where K = 0.9, λ is the wavelength of the Cu Kα radiation, β is the structural broadening of peak profile in radians, and Θ is the diffraction angle [26,27]. Hereby, for the heat treatment time 7, 9, 12 and 24 h, the average crystallites size was found to be 17, 19, 20 and 21 nm, respectively (Table 2). It might be concluded that the SrF_2 crystallites size increase gradually with the heat treatment time elongations. Additionally, the interplanar spacing *d* and the lattice parameters *a* were found using Rietveld Method. For GC370_9 and GC370_24 *d* values were found to be smaller ($d_{(111)}$ = 3.27 Å and 3.22 Å, respectively) than those of the SrF_2. The value of lattice parameters *a* changed from 5.66 Å for GC370_9 to 5.6 Å in case of GC370_24, whereas for SrF_2 *a* parameter equaled 5.79 Å. That might be attributed to the Eu^{3+} substituting Sr^{2+} during the heat treatment process. Because Eu^{3+} ions had smaller ionic radius (0.95 Å) in comparison with the Sr^{2+} ions (1.13 Å), thus the *d* value and *a* parameters decreased [28,29].

3.3. FTIR analysis

To examine the network structure of the PG and GC specimens, the FTIR spectra were obtained (shown in Fig. 4). The main feature was the wide band in the 500-850 cm^{-1} spectral range, characteristic to the tellurium based glass matrices [30]. It could be deconvoluted into three contributions. The first one at 590 cm^{-1} was due to the Te-O-Te vibrations in TeO_4 trigonal bipyramids (tbp)

Table 2
The calculated crystallite size of GC370 glass ceramics samples.

Sample	Size (nm)
GC370_7	17
GC370_9	19
GC370_12	20
GC370_24	21

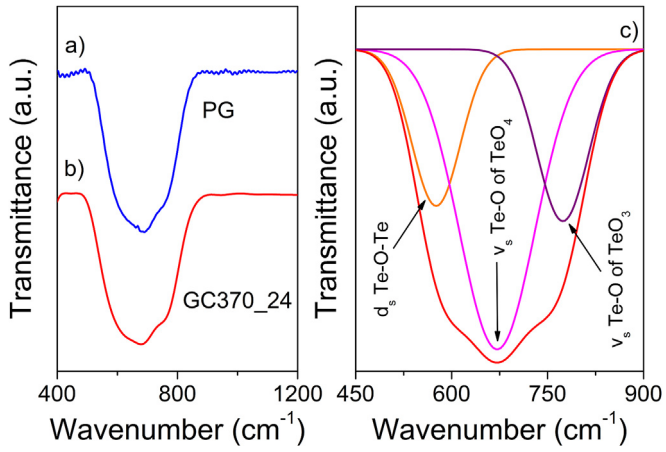

Fig. 4. FTIR spectra of PG and GC370_24.

[31]. The band at 680 cm^{-1} was ascribed to the symmetric stretching vibrations of Te-O in TeO_4 tbp units or Te-O-Te linkages between two fourfold coordinated Te atoms [32]. Finally, signal at 775 cm^{-1} had its source in the stretching vibration of Te-O in TeO_3 trigonal pyramids (tp) units and/or TeO_{3+1} polyhedral groups.

In comparison with the infrared absorption bands of the PG, the GC370_24 spectrum possessed similar character, which indicated that the crystallization process had no essential influence on the glass matrix network. These results are consistent with other reports on tellurite glass ceramics systems [33] which is satisfactory considering the fact that only SrF_2 compound was intended to form crystallites in heat treated samples. FTIR measurement confirmed that obtained tellurite based glass samples were resistant to devitrification.

3.4. XPS analysis

XPS analysis was performed to provide additional information about valance states of elements that samples were comprised of. Exemplary spectra of PG, GC370_6 and GC370_24 are presented in Fig. 5 (from top to the bottom, respectively). Fig. 5 (a) shows Eu3d region. Two peaks 1 and 2 were observed at 1132.0 and 1163.0 eV with the energy separation about 30 eV and they could be attributed to Eu^{3+} spin-orbit $3d_{5/2}$ and $3d_{3/2}$ doublet, respectively [34]. The intensities and positions of peaks assigned to Eu^{3+} remained unchanged after heat treatment procedure. Thus, it might be concluded that formation of SrF_2 nanocrystals have no influence on the oxidation state of europium.

Fig. 5 (b) shows the Sr 3d spin-orbit doublet. Peaks could be deconvoluted into four separated Gaussian-Lorentzian peaks. Apparent resolution of two Sr3d components was relatively low which indicated presence of more than one chemical state of strontium in the studied materials. Peaks 1 and 3 at energies 133.0 and 135.0 eV were attributed to the Sr $3d_{5/2}$ and Sr $3d_{3/2}$ in SrO [35,36], whereas peaks 2 and 4 at energies 133.5 and 135.5 eV corresponded to the Sr $3d_{5/2}$ and Sr $3d_{3/2}$ in SrF_2. The SrO doublet intensity decreased after crystallization process while the intensity of SrF_2 doublet peaks significantly increased for the GC370_6 and GC370_24 glass ceramics. The SrO to SrF_2 ratio varied from 1.3 for precursor glass to 0.57 and 0.33 for GC370_6 and GC370_24, respectively. Therefore, gradual transformation of SrO to SrF_2 as a result of heat treatment process has been revealed. Such results are in good agreement with the XRD measurements confirming growth of the SrF_2 nanocrystallites in glass ceramics samples after heat treatment procedure has been applied.

Moreover, in the region of 570–590 eV Te3d peak analysis has been performed (Fig. 5 (c)). Tellurium signals have been detected as a characteristic well separated spin-orbit components with peaks 2 and 4 at approximately 576.0 and 586.4 eV with distance of 10.4 eV that corresponds to TeO_2. Besides signals due to $Te3d_{5/2}$ and $Te3d_{3/2}$, low intensity features (1 and 3) are present on the low-energy side of the Te3d peaks [37]. The origin of this bands might be the presence of other tellurium based species such as TeO_3 [38]. According to our FTIR results, tellurium possess different local environments. Thus, presence of TeO_3 and TeO_4 species in the glass matrix might be the reason of additional bands appearance in the XPS spectra.

3.5. UV–Vis analysis

Optical study provided information about transitions in the UV and visible range based on observed absorption bands. The

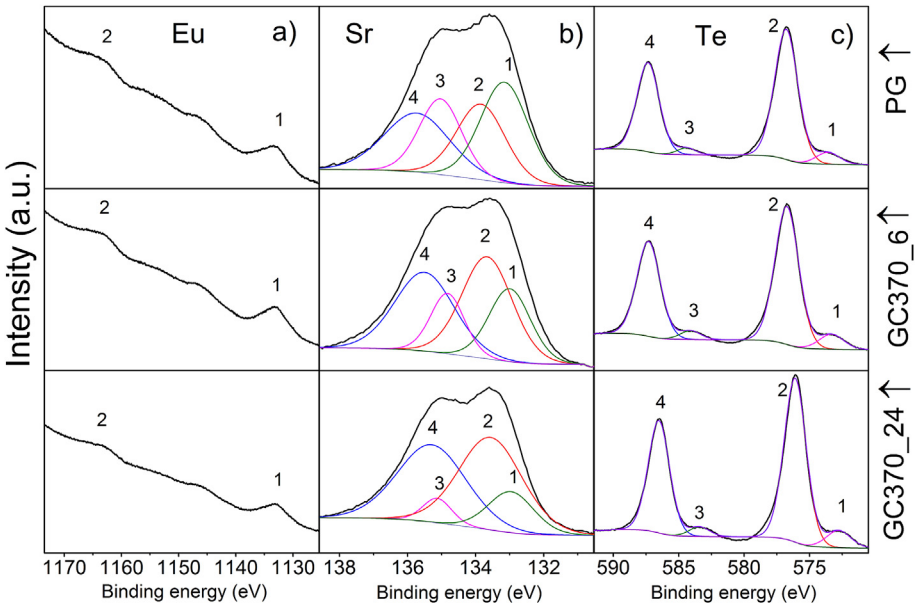

Fig. 5. XPS spectra of (a) Eu, (b) Sr, (c) Te.

absorption spectra of Eu^{3+} doped glass and glass ceramic samples in the spectral region of 380–580 nm are presented in Fig. 6. Observed bands could be ascribed to 4*f*-4*f* transitions from the $^7F_{0,1}$ levels to the excited states of Eu^{3+} ions. Three absorption bands from the $^7F_0$ ground state to the $^5D_2$ and $^5D_1$ states were present at 465 and 526 nm, respectively. Additionally, the absorption band at 535 nm due to $^7F_1 \rightarrow {}^5D_1$ transition was observed. It is well known, that transition from the first excited state ($^7F_1$) in the Eu^{3+} ions is possible due to closely spaced $^7F_0$ and $^7F_1$ states. Intensity of Eu^{3+} transitions in case of precursor glass and glass ceramics remained unchanged. Additionally, the absorption edge did not shift significantly after heat treatment procedure. Due to nanosized SrF_2 crystallites [39] transparency of glass ceramics was slightly changed, which was comparable with other results, for example [5]. Since high optical transparency is one of the most required qualities of glass ceramics systems, obtained results indicated that studied glass ceramics systems were a good candidate for RE^{3+} ions hosts.

3.6. Luminescence analysis

Luminescence properties of the precursor glass and glass ceramics doped with Eu^{3+} ions were investigated in order to determine the influence of the surroundings on luminescence intensity of Eu^{3+} ions.

Fig. 7 shows the excitation spectra of PG monitored at λ_{em} = 615 nm ($^5D_0 \rightarrow {}^7F_2$ transition of Eu^{3+} ions). Several characteristic sharp peaks originating from the 4*f*-4*f* transitions of Eu^{3+} were observable from the $^7F_0$ ground state to the excited levels: $^5D_7$ (362 nm), $^5L_7$ (382 nm), $^5L_6$ (395 nm), $^5D_3$ (416 nm) and $^5D_2$ (465 nm). Intensities of two peaks: at 395 and 465 nm were significantly higher than other peaks. Similar excitation spectra were collected in case of other samples, thus they were not presented.

Furthermore, both of the 395 and 465 nm excitation wavelengths were used to record the emission spectra of precursor glass and glass ceramics. The emission spectra excited by λ_{exc} = 395 nm (Fig. 8.) consisted of peaks due to transitions from the lowest excited states $^5D_0$ of Eu^{3+} and additionally, peaks assigned to the transitions from the highest excited states $^5D_1$ and $^5D_2$. Several peaks at 511, 535, 555, 588, 615, 653 and 703 nm were ascribed to the $^5D_2 \rightarrow {}^7F_J$ (J = 3), $^5D_1 \rightarrow {}^7F_J$ (J = 1, 2) and $^5D_0 \rightarrow {}^7F_J$ (J = 1, 2, 3, 4), respectively. For λ_{exc} = 465 nm excitation, the emission spectra of precursor glass and GC370 samples (Fig. 9.) consisted similar peaks at 535, 555, 588, 615, 653 and 703 nm. There was no significant difference on the emission intensities between precursor glass and GC360 series due to lack of crystalline phase. With the SrF_2 crystallites formation in GC370 series, the emission intensities were gradually improved. This phenomenon was related to Eu^{3+} incorporation into the SrF_2 nanocrystals during heat treatment procedure. Although tellurite glass matrices are known to have one of the lowest phonon energies among oxide glasses (about 700 cm^{-1} [40]), the SrF_2 phonon energies are considerably lower (300 cm^{-1}). In result, the non-radiative relaxation process between the Eu^{3+} excited levels $^5D_{1,2}$ and $^5D_0$ decreases and the emission from higher excited levels occurs along with Eu^{3+} luminescence increasing. Such behavior was observed only in certain low phonon glass and glass ceramics systems [41]. The overall emission color estimated based on Figs. 8 and 9 did not vary significantly for PG and GC samples. It fell in the orange region for λ_{exc} = 395 nm excitation and shifted to reddish-orange when excited by λ_{exc} = 465 nm wavelength. Emission spectra of glass specimen undoped by Eu^{3+} under both excitation wavelengths were also measured in order to estimate the influence of glass matrix on the overall emission color. It was found that pure glass matrix emitted a weak broad band in the blue spectral range thus it might slightly affected the overall color by shifting it to the lower x values. However, presence of Eu^{3+} transitions in PG and GC in the green and yellow spectrum region originating from the upper excited levels ($^5D_{1,2}$) was the predominant factor for shifting the x and y values of estimated overall emission colors from red area.

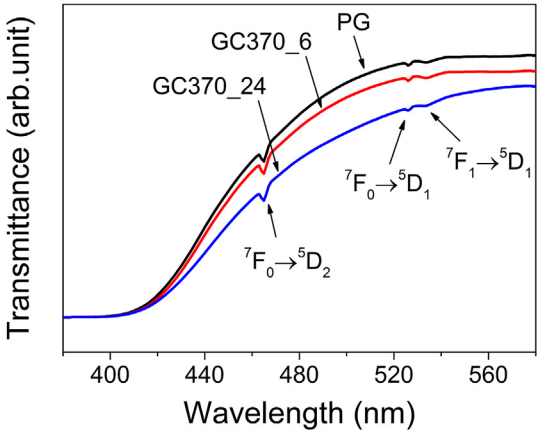

Fig. 6. UV–vis spectra of PG, GC370_6 and GC_24.

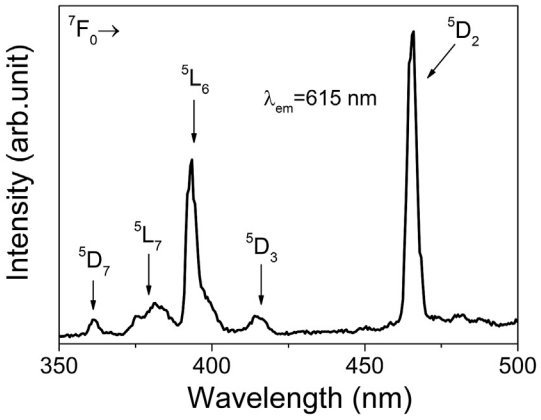

Fig. 7. Excitation spectrum of PG for λ_{em} = 615 nm.

The intensity ratio of the major emission peaks of Eu^{3+}: at 588 ($^5D_0 \rightarrow {}^7F_1$) nm and 615 nm ($^5D_0 \rightarrow {}^7F_2$) is defined as Red/Orange ratio and reflects the local surrounding symmetry of Eu^{3+} ions. It is well known, that the peak at 588 nm is due to magnetic dipole transition and does not depend on the ligand field [20]. On the other hand, peak at 615 nm originating from the forced electric dipole transition allowed only when Eu^{3+} ions occupy a site without a symmetry center [42]. Thus, the $^5D_0 \rightarrow {}^7F_2$ transition is hypersensitive to the local symmetry. Decrease of the R/O after heat treatment procedure provides an evidence of the Eu^{3+} incorporation into SrF_2 nanocrystals. The calculated R/O values were 4.84, 4.69 and 4.13 for the PC, GC370_6 and GC370_24, respectively. The continuous decrease of R/O in glass ceramics samples indicated the increasing symmetry of the ligand field of Eu^{3+} ions. Similar differences between R/O values for precursor glass and glass ceramics samples were achieved in Refs. [25] and [26]. Therefore, the Eu^{3+} enriching the SrF_2 nanocrystalline structure was confirmed, which is also consistent with XRD data analysis.

3.7. TRES analysis

TRES results provided further information concerning Eu^{3+} in the investigated glass and glass ceramics systems. The fluorescence

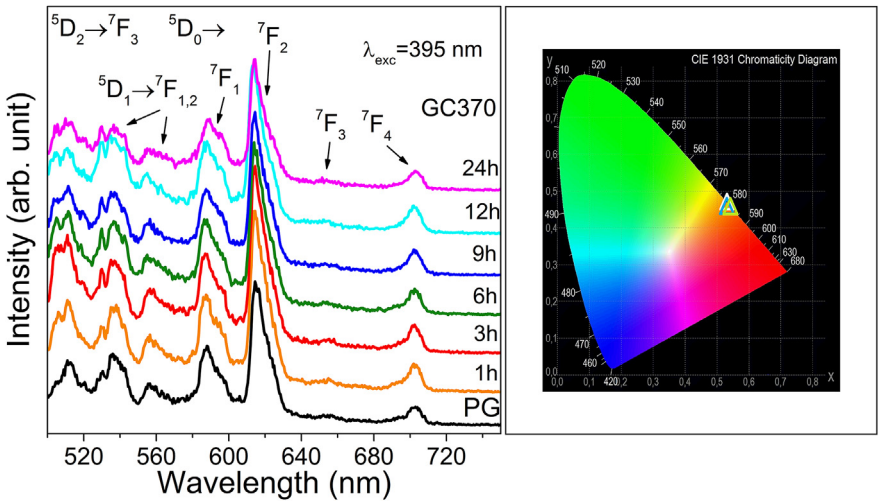

Fig. 8. Emission spectra of PG and GC370 series excited by λ_{exc} = 395 nm and CIE chromaticity diagram (white triangle represented PG, blue-GC370_6 and green-GC370_24). (For interpretation of the references to colour in this figure legend, the reader is referred to the web version of this article.)

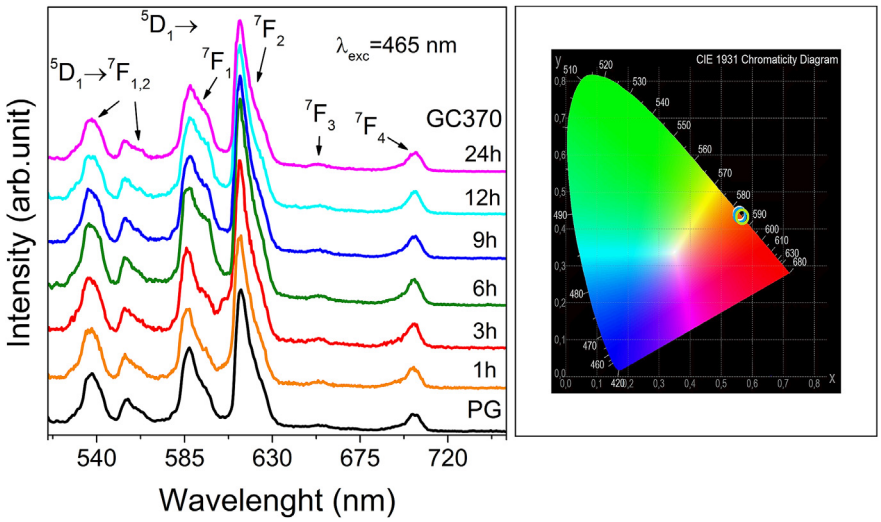

Fig. 9. Emission spectra of PG and GC370 series excited by λ_{exc} = 465 nm and CIE chromaticity diagram (white circle represented PG, blue-GC370_6 and green-GC370_24). (For interpretation of the references to colour in this figure legend, the reader is referred to the web version of this article.)

decay curves of 615 nm ($^5D_0 \rightarrow {}^7F_2$) transition of Eu^{3+} ions in PG, GC370_6 and GC370_24 samples luminescence excited by 465 nm wavelength are shown in Fig. 10.

The double-exponential character of the decay curves indicated presence of two different surroundings of Eu^{3+} ions. Long lifetimes (τ_1) are correlated with the higher symmetry of the crystal field, whereas the short lifetimes (τ_2) are connected with the lower symmetry of Eu^{3+} surroundings [21]. In case of measured samples, τ_1 represented the lifetime of Eu^{3+} incorporated into the SrF_2 nanocrystals while τ_2 was due to Eu^{3+} in the glass matrix. Based on the collected data, the Eu^{3+} 615 nm calculated average fluorescence decay lifetimes in glass ceramics for both, the GC370_6 and GC370_24 were slightly longer (τ = 0.68 and 0.73 ms, respectively) comparing to the PG (τ = 0.67 ms). The relatively low differences between measured lifetimes comparison to other publications [21,25,43] might be explained as follows: Eu^{3+} ions partially enriched the SrF_2 crystal lattice, however some of the Eu^{3+} ions also remained in glass matrix. Similar results were obtained by de Pablos-Martin et al. [44]. They found that for aluminosilicate

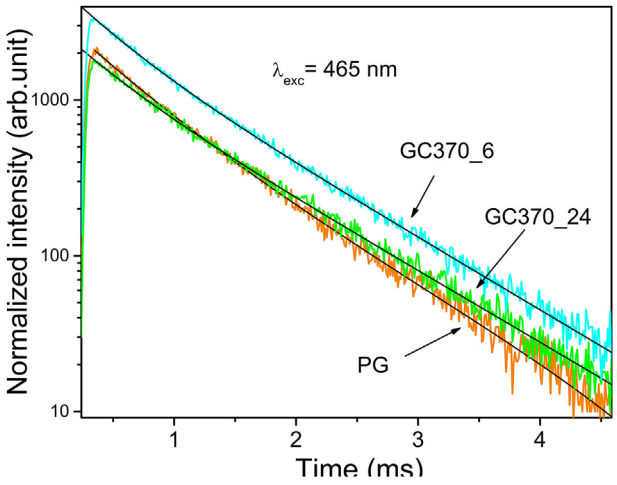

Fig. 10. TRES of PG, GC370_6 and GC370_24 for 615 nm observation with the excitation wavelength λ_{exc} = 465 nm.

glasses thulium was present in both, the glass matrix and nanocrystalline LaF_3.

Therefore, along with the presented luminescence results for GC370 series it might be concluded that Eu^{3+} incorporation in the SrF_2 nanocrystals is an advantage in terms of efficiency improvement of investigated materials for LED phosphors applications.

4. Conclusions

Eu^{3+} doped tellurite glass ceramics containing SrF_2 nanocrystals were successfully synthesized. Formation of SrF_2 crystallites was confirmed by XRD patterns and the presence of the Sr-F bonds was detected by XPS. The size of crystallites in range 17–21 nm was controlled by modifying the heat treatment duration. Part of Eu^{3+} ions enriched the SrF_2 crystal lattice which was observed at luminescence results such as R/O ratio and fluorescence decay lifetimes which depended on the Eu^{3+} local symmetry of surrounding environment. For glass ceramics samples, the R/O ratio decreased subsequently with the heat treatment time increase because the intensity of the electric $^5D_0 \rightarrow {}^7F_2$ transition is related with Eu^{3+} occupying the non-inversion symmetry positions, whereas the magnetic dipole $^5D_0 \rightarrow {}^7F_1$ transition reflects the Eu^{3+} position with the inversion symmetry in SrF_2 crystal structure. The Eu^{3+} average decay lifetimes were slightly longer for glass ceramics in comparison with precursor glass due to Eu^{3+} location partially in higher symmetry surroundings. Because of low-phonon energy environment, transitions from the Eu^{3+}: $^5D_0$ as well as $^5D_{1,2}$ levels were observed. The highest emission intensity of Eu^{3+} was monitored in GC 370_6 sample. Presented study suggests that tellurite glass ceramics containing SrF_2 nanocrystals are excellent hosts for Eu^{3+} ions. Moreover, obtained results allowed to determine optimal parameters of heat treatment procedure to enhance the Eu^{3+} luminescence properties and therefore gave a possibility for further investigation of described GC doped by various RE^{3+} ions in order to achieve white light emission. Such materials might find application in photonics for example as a LED and WLED phosphors.

Acknowledgements

This research has been supported by the grant 2015/17/B/ST5/03143 financed by National Science Centre (A. Synak).

References

[1] Q. Wang, S. Ouyang, W. Zhang, B. Yang, Y. Zhang, H. Xia, Luminescent properties of Ce3+ -doped transparent oxyfluoride glass ceramics containing BaGdF5 nanocrystals, J. Rare Earths 33 (2015) 13–19, http://dx.doi.org/10.1016/S1002-0721(14)60376-8.

[2] X. Qiao, X. Fan, Z. Xue, X. Xu, Q. Luo, Intense ultraviolet upconversion luminescence of Yb3+ and Tb3+ co-doped glass ceramics containing SrF2 nanocrystals, J. Lumin. 131 (2011) 2036–2041, http://dx.doi.org/10.1016/j.jlumin.2011.05.012.

[3] P. Gredin, M. Mortier, A.J. Stevenson, Fluoride Materials for Optical Applications: Single Crystals, Ceramics, Glasses, and Glass – Ceramics, vol. 132, 2011, pp. 1165–1173, http://dx.doi.org/10.1016/j.jfluchem.2011.07.017.

[4] S. Bae, Y. Gyu, W. Bin, K. Seok, W. Jin, Rare earth doped silicate-oxyfluoride glass ceramics incorporating LaF3 nano-crystals for UV-LED color conversion, Opt. Mater. Amst. 35 (2013) 2034–2038, http://dx.doi.org/10.1016/j.optmat.2012.09.025.

[5] X. Wang, J. Chen, J. Li, H. Guo, Preparation and luminescent properties of Eu-doped transparent glass-ceramics containing SrF2 nanocrystals, J. Non. Cryst. Solids 357 (2011) 2290–2293, http://dx.doi.org/10.1016/j.jnoncrysol.2010.11.068.

[6] A.M. Babu, B.C. Jamalaiah, T. Suhasini, T.S. Rao, L.R. Moorthy, Optical properties of Eu 3+ ions in lead tungstate tellurite glasses, Solid State Sci. 13 (2011) 574–578, http://dx.doi.org/10.1016/j.solidstatesciences.2010.12.028.

[7] R. Wang, D. Zhou, J. Qiu, Y. Yang, C. Wang, Color-tunable luminescence in Eu3+/Tb3+ co-doped oxyfluoride glass and transparent glass–ceramics, J. Alloys Compd. 629 (2015) 310–314, http://dx.doi.org/10.1016/j.jallcom.2014.12.233.

[8] Q. Luo, X. Qiao, X. Fan, X. Zhang, Preparation and luminescence properties of Ce3+ and Tb 3+ co-doped glasses and glass ceramics containing SrF 2 nanocrystals, J. Non. Cryst. Solids 356 (2010) 2875–2879, http://dx.doi.org/10.1016/j.jnoncrysol.2010.09.018.

[9] X. Qiao, X. Fan, Z. Xue, X. Xu, Q. Luo, Upconversion luminescence of Yb3+/Tb3+/Er3+ -doped fluorosilicate glass ceramics containing SrF2 nanocrystals, J. Alloys Compd. 509 (2011) 4714–4721, http://dx.doi.org/10.1016/j.jallcom.2011.01.099.

[10] S. Ye, Y. Katayama, S. Tanabe, Down conversion luminescence of Tb3+ –Yb3+ codoped SrF2 precipitated glass ceramics, J. Non. Cryst. Solids 357 (2011) 2268–2271, http://dx.doi.org/10.1016/j.jnoncrysol.2010.11.083.

[11] A. Fedotovs, A. Antuzevics, U. Rogulis, M. Kemere, R. Ignatans, Electron paramagnetic resonance and magnetic circular dichroism of Gd3+ ions in oxy fluoride glass – ceramics containing CaF2 nanocrystals, J. Non. Cryst. Solids 429 (2015) 118–121, http://dx.doi.org/10.1016/j.jnoncrysol.2015.08.036.

[12] W. Huiyun, Y.E. Song, L.I.U. Tianhua, L.I. Song, H.U. Rongxuan, Influence of local phonon energy on quantum efficiency of Tb3+ -Yb3+ co-doped glass ceramics containing fluoride nanocrystals, J. Rare Earths 33 (2015) 524–528, http://dx.doi.org/10.1016/S1002-0721(14)60451-8.

[13] W. Wang, X. Lei, H. Gao, Y. Mao, Near-infrared quantum cutting platform in transparent oxyfluoride glass – ceramics for solar cells, Opt. Mater. Amst. 47 (2015) 270–275, http://dx.doi.org/10.1016/j.optmat.2015.05.040.

[14] Y. Yu, D. Chen, Y. Wang, F. Liu, E. Ma, A new transparent oxyfluoride glass ceramic with improved luminescence, J. Non. Cryst. 353 (2007) 405–409, http://dx.doi.org/10.1016/j.jnoncrysol.2006.12.029.

[15] L. Zur, J. Janek, E. Pietrasik, M. So, J. Pisarska, W.A. Pisarski, Influence of MO/MF2 Modifiers (M ¼ Ca, Sr, Ba) on Spectroscopic Properties of Eu3+ Ions in Germanate and Borate Glasses, 2016, pp. 3–7, http://dx.doi.org/10.1016/j.optmat.2016.05.045.

[16] Y. He, G. Zhao, H. Qin, J. Wang, G. Han, Photoluminescence properties of Dy3+ -doped oxy fluoride germanosilicate optical glass-ceramics, Opt. Commun. 315 (2014) 59–62, http://dx.doi.org/10.1016/j.optcom.2013.10.083.

[17] Q. Luo, X. Qiao, X. Fan, S. Liu, H. Yang, X. Zhang, Reduction and luminescence of europium ions in glass ceramics containing SrF2 nanocrystals, J. Non. Cryst. 354 (2008) 4691–4694, http://dx.doi.org/10.1016/j.jnoncrysol.2008.07.019.

[18] M.H. Imanieh, I.R. Martín, A. Nadarajah, J.G. Lawrence, V. Lavín, J. González-platas, Upconversion emission of a novel glass ceramic containing Er3+, Yb3+: Sr1-xYxF2+x nano-crystals, J. Lumin. 172 (2016) 201–207, http://dx.doi.org/10.1016/j.jlumin.2015.12.026.

[19] Z. Hou, Z. Xue, S. Wang, Synthesis and spectroscopic properties of Er3+-doped CaF2 nanocrystals in transparent oxyfluoride tellurite glass–ceramics, J. Alloys Compd. 514 (2012) 109–112, http://dx.doi.org/10.1016/j.jallcom.2011.11.013.

[20] B. Grobelna, P. Bojarski, B. Kuklinski, A.A. Kubicki, A. Synak, Optical properties and luminescence kinetics of Ln1.9Pr0.1(WO4)3 (where Ln = Gd, La) immobilized in silica xerogel, Opt. Mater. 34 (2011) 103–108, http://dx.doi.org/10.1016/j.optmat.2011.07.011.

[21] M. Saad, M. Poulain, Glass forming ability criterion, Mater. Sci. Forum 19/20 (1987) 11–18.

[22] Y. Tian, B. Li, R. Chen, J. Xia, X. Jing, J. Zhang, et al., Thermal stability and 2.7 μm spectroscopic properties in Er3+ doped tellurite glasses, Solid State Sci. 60 (2016) 17–22, http://dx.doi.org/10.1016/j.solidstatesciences.2016.07.012.

[23] C. Paßlick, B. Ahrens, B. Henke, J.A. Johnson, S. Schweizer, Differential scanning calorimetry investigations on Eu-doped fluorozirconate-based glass ceramics, J. Non. Cryst. Solids 356 (2010) 3085–3089, http://dx.doi.org/10.1016/j.jnoncrysol.2010.02.025.

[24] A. Hrubý, Evaluation of glass-forming tendency by means of DTA, Czechoslov. J. Phys. 22 (1972) 1187–1193, http://dx.doi.org/10.1007/BF01690134.

[25] H. Jin, Z. Mo, X. Zhang, L. Yuan, M. Yan, L. Li, Luminescent properties of Eu3+ -doped glass ceramics containing BaCl2 nanocrystals under NUV excitation for White LED, J. Lumin. 175 (2016) 187–192, http://dx.doi.org/10.1016/j.jlumin.2016.03.002.

[26] A. Dwivedi, C. Joshi, S.B. Rai, Effect of heat treatment on structural, thermal and optical properties of Eu3+ doped tellurite glass: formation of glass-ceramic and ceramics, Opt. Mater. Amst. 45 (2015) 202–208, http://dx.doi.org/10.1016/j.optmat.2015.03.038.

[27] H. Karimi, Y. Zhang, S. Cui, R. Ma, G. Li, Q. Wang, et al., Spectroscopic properties of Eu-doped oxynitride glass – ceramics for white light LEDs, J. Non. Cryst. Solids 406 (2014) 119–126, http://dx.doi.org/10.1016/j.jnoncrysol.2014.10.003.

[28] Q. Feng, J. Guo, X. Xu, H. Zhang, X. Zhu, S. Feng, The effect of ionic radius of metal element (M) on (Pb,M)- 1212 superconductors (M= Sr. Ca, Mg, Hg, Cd, Cu), Solid State Com. 94 (1995) 21–25, http://dx.doi.org/10.1016/0038-1098(95)00019-4.

[29] P. Ganguly, Influence of ionic radius of rare-earths on the structural and electrical properties of Ba 5RTi3Nb7O30 (R = rare-earth) ferroelectric ceramics, J. Rare Earths 33 (2015) 1310–1315, http://dx.doi.org/10.1016/S1002-0721(14)60562-7.

[30] P.G. Pavani, K. Sadhana, V.C. Mouli, Optical, physical and structural studies of boro-zinc tellurite glasses, Phys. B Phys. Condens. Matter 406 (2011) 1242–1247, http://dx.doi.org/10.1016/j.physb.2011.01.006.

[31] M.S. Sajna, S. Thomas, C. Jayakrishnan, C. Joseph, P.R. Biju, N.V. Unnikrishnan, NIR emission studies and dielectric properties of Er3+ -doped multicomponent tellurite glasses, Spectrochim. Acta Part A 161 (2016) 130–137, http://dx.doi.org/10.1016/j.saa.2016.02.039.

[32] N. Jaba, Raman spectroscopy studies of Er3+ -doped zinc tellurite glasses, J. Non. Cryst. Solids 351 (2005) 833–837, http://dx.doi.org/10.1016/

j.jnoncrysol.2005.02.003.
[33] M.Y.A. Yagoub, H.C. Swart, L.L. Noto, J.H.O. Connel, M.E. Lee, E. Coetsee, The effects of Eu-concentrations on the luminescent properties of SrF2: Eu nanophosphor, J. Lumin. 156 (2014) 150–156, http://dx.doi.org/10.1016/j.jlumin.2014.08.014.
[34] Wagner, et al., Handbook of X-Ray Photoelectron Spectroscopy, Perkin-Elmer, 1979.
[35] M.Y.A. Yagoub, H.C. Swart, E. Coetsee, Concentration quenching, surface and spectral analyses of SrF2: Pr3+ prepared by different synthesis techniques, Opt. Mater. Amst. 42 (2015) 204–209, http://dx.doi.org/10.1016/j.optmat.2015.01.011.
[36] G.D. Khattak, A. Mekki, L.E. Wenger, Local structure and redox state of copper in tellurite glasses, J. Non. Cryst. Solids 337 (2004) 174–181, http://dx.doi.org/10.1016/j.jnoncrysol.2003.08.088.
[37] A. Mekki, G.D. Khattak, L.E. Wenger, XPS and magnetic studies of vanadium tellurite glassses, J. Electron Spectrosc. Relat. Phenom. 175 (2009) 21–26, http://dx.doi.org/10.1016/j.elspec.2009.07.001.
[38] M. Secu, C.E. Secu, Up-conversion luminescence of Er3+/Yb3+ co-doped LiYF4 nanocrystals in sol – gel derived oxy fluoride glass-ceramics, J. Non. Cryst. Solids 426 (2015) 78–82, http://dx.doi.org/10.1016/j.jnoncrysol.2015.07.010.
[39] M. Reben, The thermal study of oxyfluoride glass with strontium fluoride, J. Non. Cryst. Solids 357 (2011) 2653–2657, http://dx.doi.org/10.1016/j.jnoncrysol.2010.12.055.
[40] W. Stambouli, H. Elhouichet, B. Gelloz, M. Fe, Optical and Spectroscopic Properties of Eu-doped Tellurite Glasses and Glass Ceramics, vol. 138, 2013, pp. 201–208, http://dx.doi.org/10.1016/j.jlumin.2013.01.019.
[41] A. Kumar, D.K. Rai, S.B. Rai, Optical Studies of Eu3+ Ions Doped in Tellurite Glass, vol. 58, 2002, pp. 2115–2125.
[42] R. Narro-garcía, H. Desirena, T. López-luke, J. Guerrero-contreras, C.K. Jayasankar, Spectroscopic Properties of Eu3+/Nd3+ Co-doped Phosphate Glasses and Opaque Glass – Ceramics, vol. 46, 2015, pp. 34–39, http://dx.doi.org/10.1016/j.optmat.2015.03.051.
[43] Y. Fei, S. Zhao, X. Sun, L. Huang, D. Deng, S. Xu, Preparation and optical properties of Eu3+ doped and Er3+/Yb3+ codoped oxyfluoride glass ceramics containing Ba1−x LuxF2+x nanocrystals, J. Non. Cryst. Solids 428 (2015) 20–25, http://dx.doi.org/10.1016/j.jnoncrysol.2015.08.004.
[44] A. de Pablos-Martin, C. Patzig, T. Höche, A. Duran, M.J. Pascual, Distribution of thulium in Tm3+-doped oxyfluoride glasses and glass-ceramics, CrystEngComm 15 (2013) 6979, http://dx.doi.org/10.1039/c3ce40731d.